

## Transport theory of metallic *B20* helimagnets

Jian Kang<sup>1,\*</sup> and Jiadong Zang<sup>2,†</sup>

<sup>1</sup>*School of Physics and Astronomy, University of Minnesota, Minneapolis, Minnesota 55455, USA*

<sup>2</sup>*Department of Physics and Astronomy, Johns Hopkins University, Baltimore, Maryland 21218, USA*

(Received 20 December 2014; published 1 April 2015)

*B20* compounds are a class of cubic helimagnets harboring nontrivial spin textures such as spin helices and skyrmions. It has been well understood that the Dzyaloshinskii-Moriya (DM) interaction is the origin of these textures, and the physics behind the DM interaction is the spin-orbit coupling (SOC). However, the SOC shows its effect not only on the spins but also on the electrons. In this paper, we will discuss the effects of the SOC on the electron and spin transports in *B20* compounds. An effective Hamiltonian is presented from symmetry analysis, and the spin-orbit coupling therein shows anomalous behaviors in anisotropic magnetoresistance and helical resistance. New effects such as an inverse spin-galvanic effect are proposed, and the origin of the DM interaction is discussed.

DOI: [10.1103/PhysRevB.91.134401](https://doi.org/10.1103/PhysRevB.91.134401)

PACS number(s): 71.10.Ay, 72.10.Fk, 72.15.Gd, 75.10.Hk

### I. INTRODUCTION

Symmetry is a central topic of modern physics and material science. Reduced symmetry has given rise to innumerable novel phenomena. For example, breaking of the translational symmetry leads to the emergence of lattices and crystals, which are the platforms of condensed-matter studies. The highest symmetry of a lattice has the point group of  $O_h$ , to which most of the ferromagnetic materials belong. Surprises have been brought by further reducing this symmetry. *B20* compounds, with representatives of FeSi [1,2], MnSi [3–5], FeGe [6,7], and Cu<sub>2</sub>SeO<sub>3</sub> [8], are such an interesting class of materials. Although *B20* compounds have a cubic lattice, it has the lowest symmetry in this crystal system. Complicated distributions of atoms dramatically bring down the symmetry, where inversion, mirror, or fourfold rotational symmetries are absent. Abundant phenomena are emerging consequently, among which the most attractive one is the presence of nontrivial spin textures like helices and skyrmions.

A spin helix is a spatially modulated magnetic texture. It is present in magnetic materials with competing interactions. It has been observed in the *B20* family Fe<sub>1-x</sub>Co<sub>x</sub>Si by real-space imaging [9]. In this case, the Dzyaloshinskii-Moriya (DM) interaction [10,11]

$$H_{DM} = \mathbf{D} \cdot (\mathbf{S}_i \times \mathbf{S}_j) \quad (1)$$

between neighboring spins plays an important role. Broken inversion symmetry in *B20* compounds is the physical origin of this interaction. Under an inversion operation about the center of the joint line, two neighboring spins are exchanged, and the DM interaction flips sign due to its cross-product nature. In contrast, the Heisenberg exchange,  $H_H = -\mathbf{J}\mathbf{S}_i \cdot \mathbf{S}_j$ , is unchanged under this operation, thus respecting the inversion symmetry. The Heisenberg exchange tends to align neighboring spins, while the DM interaction tends to form an angle of  $\pi/2$ . As a result of the competition, a finite angle is expanded by these two spins, whose successive arrangement generates the spin helix. A spin helix is not the

only result of breaking inversion symmetry; another result is the magnetic skyrmion [3,12–14], a topological spin texture. It is stabilized in *B20* compounds at finite magnetic fields and temperatures.

In light of nontrivial spin modulation in the helix and promising spintronics applications of the skyrmion, a complete understanding of the electron and spin transports in *B20* compounds is an urgent subject. Longitudinal magnetoresistance measurements have been performed to map out the phase diagrams containing helical and skyrmion phases [15,16]. On the other hand, due to the emergent electromagnetism [17,18], the skyrmion phase can be precisely determined by the Hall measurements [6,19–22]. A peculiar non-Fermi-liquid behavior is also addressed in MnSi single crystals [4,5] and is intimately related to the topology of spin textures [23]. However, a deep study of the spin transports in *B20* compounds is still lacking. Recently, an experiment on anisotropic magnetoresistance (AMR) was performed in bulk samples of Fe<sub>1-x</sub>Co<sub>x</sub>Si [24]. It was surprisingly observed that compared to the usual AMR in cobalt or other cubic ferromagnetic materials, the magnetoresistance shows two, instead of four, peaks. This result shows that the system lacks the fourfold rotational symmetry, which is compatible with the reduced symmetry in *B20* compounds. However, the microscopic origin has yet to be revealed. In another experiment, the measurement of helical resistance showed an ultralow resistance ratio of 1.35 with the current parallel and perpendicular to the helix [25]. It was predicted theoretically and well tested experimentally that this ratio should be larger than 3. This observation apparently violates this common concept.

These two experiments suggest a new mechanism involving nontrivial spin scatterings and thus inevitably suggest the important effects of the spin-orbit coupling (SOC) on the conduction electrons in *B20* compounds. The SOC has already shown its power in the spin interactions in *B20* compounds. It is well known that a nonvanishing DM interaction requires not only the inversion symmetry breaking but also a large SOC [11]. However, effects of the SOC on conduction electrons have never been discussed. In this paper, we will show that the SOC explains well the two experiments above and provides several other experimental proposals.

\*jkang@umn.edu

†jiadongzang@gmail.com

This paper is organized as follows. In the following section, an effective Hamiltonian is constructed, where both linear and cubic SOC terms are present. Section III shows that these SOC terms are the microscopic origin of the DM interactions in *B20* compounds. In Secs. IV and V, the linear SOC gives rise to an inverse spin-galvanic effect and an ultralow ratio of helical resistance, respectively. In Sec. VI, the importance of the cubic SOC is revealed, which provides the microscopic mechanism of the anomalous AMR effect.

## II. EFFECTIVE HAMILTONIAN

In order to understand the transport behaviors of *B20* compounds, the first priority is to construct the effective Hamiltonian of the conduction electrons. As we are interested in the long-range behaviors, only momenta around the  $\Gamma$  point will be relevant. The bands around other high-symmetry points in the Brillouin zone might cross the Fermi energy and contribute to the transports in some form. However, the qualitative behavior, especially the symmetries, will not change.

The importance of the SOC indicates that the conventional quadratic dispersion,  $H(\mathbf{k}) = \hbar^2 \mathbf{k}^2 / 2m$ , is not adequate to understand spin-related transports. Therefore, additional terms coupling spin and momentum are called for. To this end, we analyze the symmetry of the *B20* compounds and employ the theory of invariants to construct the effective Hamiltonian [26].

In the international notation, the space group of *B20* compounds is  $P_{213}$ , where subscripts 2 and 3 indicate the twofold and threefold rotational symmetries, respectively, while 1 indicates a fractal translation in the space-group operation. No other symmetries are present. Around the  $\Gamma$  point, the fractal rotation does not change the space-group irreducible representations [27] and thus is not relevant, and the space group is isomorphic to its  $K$  group, which is a group containing all the point-group operations within the space group. Irreducible representations of the space group at the  $\Gamma$  point are the same as those of the  $K$  group. For  $P_{213}$ , the  $K$  group is the  $T23$  group, containing 12 elements: one identity, three  $C_2$  rotations ( $\pi$  rotations about axes [100], [010], and [001]), and eight  $C_3$  rotations (clockwise rotations of  $2\pi/3$  about the directions  $[\pm 1, \pm 1, \pm 1]$ ). Unlike in the complete group operations in the  $O_h$  group, fourfold rotations, inversions, and mirror symmetries are absent.

Once spin is taken into account, a  $2\pi$  rotation in the spin space reverses the sign and should be treated as an additional group operation. One thus has to consider the double group of  $T23$ , whose irreducible representations and characters are listed in Table I. Operations with bars are the joint action of the point-group element and the  $2\pi$  spin rotation.

First-principles calculations on metallic *B20* materials, such as MnSi and FeGe, show that the orbitals around the Fermi surface are mainly *d* orbitals [28]. Under spin-orbit coupling, these orbitals are split into  $j = 5/2$  and  $j = 3/2$  orbitals, which correspond to the  $D_{5/2}$  and  $D_{3/2}$  irreducible representations of the rotation group, respectively. The character of a rotation of angle  $\alpha$  in  $D_j$  is given by

$$\chi = \frac{\sin[(j + \frac{1}{2})\alpha]}{\sin(\frac{1}{2}\alpha)}. \quad (2)$$

TABLE I. Character table for the double group of  $T23$ .

$T23$	$E$	$\bar{E}$	$4C_3$	$4\bar{C}_3$	$3C_2 + 3\bar{C}_2$	$4C_3^{-1}$	$4\bar{C}_3^{-1}$
$\Gamma_1$	1	1	1	1	1	1	1
$\Gamma_2$	1	1	$w$	$w$	1	$w^2$	$w^2$
$\Gamma_3$	1	1	$w^2$	$w^2$	1	$w$	$w$
$\Gamma_4$	3	3	0	0	-1	0	0
$\Gamma_5$	2	-2	1	-1	0	1	-1
$\Gamma_6$	2	-2	$w$	$-w$	0	$w^2$	$-w^2$
$\Gamma_7$	2	-2	$w^2$	$-w^2$	0	$w$	$-w$

In the crystal field, these orbitals are further split into suborbitals, which corresponds to the decomposition in terms of  $T23$ 's irreducible representations:

$$D_{5/2} \downarrow T = \Gamma_5 \oplus \Gamma_6 \oplus \Gamma_7, \quad (3)$$

$$D_{3/2} \downarrow T = \Gamma_6 \oplus \Gamma_7. \quad (4)$$

In reality, all these suborbitals might be relevant around the Fermi surface. In addition, there are four magnetic atoms in each unit cell, leading to a total of 20 bands. In order to capture the key feature of these materials, we would like to keep the Hamiltonian in the minimal form. Only one band out of three representations  $\Gamma_{5,6,7}$  will be considered. The resulting Hamiltonian will be  $2 \times 2$ , the simplest Hamiltonian taking into account the SOC.

The model Hamiltonian  $H$  communicating the Hilbert spaces corresponding to irreducible representations  $\alpha$  and  $\beta$  is, in general,

$$H(\mathbf{k}) = \sum_{l_1^\alpha=1}^{n_\alpha} \sum_{l_2^\beta=1}^{n_\beta} h(\mathbf{k}) |l_1^\alpha\rangle \langle l_2^\beta|. \quad (5)$$

Here  $n_\alpha$  and  $n_\beta$  are dimensions of these two representations, respectively. In the current case, band mixing is neglected such that  $\alpha = \beta$ .  $l_1^\alpha$  labels the basis in the irreducible representation  $\alpha$ . The operator part  $|l_1^\alpha\rangle \langle l_2^\beta|$  transforms as the product representation  $\Gamma_\alpha^* \times \Gamma_\beta$ , which can be decomposed as the direct sum of irreducible representations  $\Gamma_\alpha^* \times \Gamma_\beta = \bigoplus_\gamma \Gamma_\gamma$ . The basis  $X_{l_3^\gamma}^\gamma$  of an irreducible representation  $\Gamma_\gamma$  contained in this product representation is the superposition of direct products  $|l_1^\alpha\rangle \langle l_2^\beta|$  as  $X_{l_3^\gamma}^\gamma = \sum_{l_1^\alpha=1}^{n_\alpha} \sum_{l_2^\beta=1}^{n_\beta} C_{l_1^\alpha l_2^\beta l_3^\gamma}^{\alpha\beta,\gamma} |l_1^\alpha\rangle \langle l_2^\beta|$ , where  $C_{l_1^\alpha l_2^\beta l_3^\gamma}^{\alpha\beta,\gamma}$  are the Clebsch-Gordan coefficients [29]. To keep the Hamiltonian invariant under group operations,  $h(\mathbf{k})$  must be an irreducible tensor operator in the representation  $\Gamma_\gamma^*$ , such that  $H(\mathbf{k})$  belongs to the trivial representation  $\Gamma_1$  contained in the product representation  $\Gamma_\gamma^* \times \Gamma_\gamma$ . As a consequence, the invariant Hamiltonian is given by

$$H(\mathbf{k}) = \sum_\gamma a_\gamma^{\alpha\beta} \sum_1^{n_\gamma} h_{l_3^\gamma}^\gamma(\mathbf{k}) X_{l_3^\gamma}^\gamma \quad (6)$$

$$= \sum_\gamma a_\gamma^{\alpha\beta} \sum_1^{n_\gamma} h_{l_3^\gamma}^\gamma(\mathbf{k}) \left( \sum_{l_1^\alpha=1}^{n_\alpha} \sum_{l_2^\beta=1}^{n_\beta} C_{l_1^\alpha l_2^\beta l_3^\gamma}^{\alpha\beta,\gamma} |l_1^\alpha\rangle \langle l_2^\beta| \right), \quad (7)$$

where coefficients  $a_{\gamma}^{\alpha\beta}$  are free parameters that cannot be dictated from the symmetry analysis.

For  $\Gamma_5$ ,  $\Gamma_5^* \times \Gamma_5 = \Gamma_1 \oplus \Gamma_4$ . However,  $X_1^{\Gamma_1}$  and all three matrices  $X_{1,2,3}^{\Gamma_4}$  are all trivial identity matrices. Therefore, the effective Hamiltonian can be reduced to be spinless, and spin-orbit coupling is absent. The corresponding Hamiltonian is therefore the simplest quadratic one,  $H(\mathbf{k}) = \hbar^2 \mathbf{k}^2 / 2m$ , which does not bring anything new. New physics comes when we turn to  $\Gamma_6$  or  $\Gamma_7$  representations. As these two representations are complex conjugate to each other, the effective Hamiltonians are the same. In the following, we will take  $\Gamma_6$  as an example without loss of generality.

$$\Gamma_6^* \times \Gamma_6 = \Gamma_1 \oplus \Gamma_4, \quad (8)$$

$$X_1^{\Gamma_1} = \begin{pmatrix} 1 & 0 \\ 0 & 1 \end{pmatrix}, \quad X_1^{\Gamma_4} = \begin{pmatrix} 0 & -i/\sqrt{3} \\ -i/\sqrt{3} & 0 \end{pmatrix},$$

$$X_2^{\Gamma_4} = \begin{pmatrix} 0 & 1/\sqrt{3} \\ -1/\sqrt{3} & 0 \end{pmatrix}, \quad X_3^{\Gamma_4} = \begin{pmatrix} -i/\sqrt{3} & 0 \\ 0 & i/\sqrt{3} \end{pmatrix}. \quad (9)$$

Equation (9) shows explicitly that  $X_i^{\Gamma_4} = -i/\sqrt{3}\sigma_i$ , where  $\sigma_i$  are three Pauli matrices. The overall factor  $-i/\sqrt{3}$  can be absorbed into the factor  $a_{\gamma}^{\alpha\beta}$  in Eq. (7). Now the remaining task is to construct the irreducible tensor operators  $h_{l_3}^{\gamma}(\mathbf{k})$ . For  $\Gamma_1$ , the task is simple because  $h_1^{\Gamma_1}(\mathbf{k}) = \mathbf{k}^2 / 2m$ . However, for  $\Gamma_4$ , two bases may apply:  $h_i^{\Gamma_4}(\mathbf{k}) = (k_x, k_y, k_z)$  or  $h_i^{\Gamma_4} = (k_x(k_y^2 - k_z^2), k_y(k_z^2 - k_x^2), k_z(k_x^2 - k_y^2))$ , which are on the first and third orders in momentum  $\mathbf{k}$ , respectively. Terms of second order in  $\mathbf{k}$  break the time-reversal symmetry once coupled to the spin and thus can be neglected. As a consequence, the effective Hamiltonian for conduction electrons in *B20* compounds is given by

$$H = \frac{\mathbf{k}^2}{2m} + \alpha(k_x\sigma_x + k_y\sigma_y + k_z\sigma_z) + \beta[k_x\sigma_x(k_y^2 - k_z^2) + k_y\sigma_y(k_z^2 - k_x^2) + k_z\sigma_z(k_x^2 - k_y^2)]. \quad (10)$$

This Hamiltonian can also be intuitively guessed from simple symmetry analysis. The presence of  $C_3$  symmetry enforces the permutation symmetry in the Hamiltonian, while the  $C_2$  symmetry rules out most of the combinations. It is worth emphasizing that the linear spin-orbit coupling  $\mathbf{k} \cdot \boldsymbol{\sigma}$  is not adequate, as it is a fully rotational symmetric term.  $C_4$  symmetry is also respected by this term but is apparently broken in the *T23* group. It is the cubic spin-orbit coupling, the last term in Eq. (10), that breaks  $C_4$ . Therefore, Eq. (10) is the minimal Hamiltonian that faithfully describes the symmetry of *B20* compounds.

The cubic spin-orbit coupling is well known in III-V semiconductors induced by bulk inversion asymmetry (BIA) [30]. The linear term  $\mathbf{k} \cdot \boldsymbol{\sigma}$  is a new term. As discussed in the following, it captures most of the nontrivial physics in *B20* compounds. As  $\boldsymbol{\sigma}$  is a pseudovector,  $\mathbf{k} \cdot \boldsymbol{\sigma}$  is a pseudoscalar. This is thus a forbidden term in lattices with any inversion

or mirror symmetries. That is why it is absent in the III-V semiconductors and most of the ferromagnetic materials. However, elements in the *T23* point group are only pure rotations, so  $\mathbf{k} \cdot \boldsymbol{\sigma}$  is allowed and contributes significantly to the long-range behaviors.

### III. ORIGIN OF SPIN INTERACTIONS

Real-space images of *B20* compounds have shown that the spin helix therein looks like a successive array of Bloch walls [9], where magnetizations are rotating in a plane perpendicular to their propagation direction. In addition, the skyrmion has a double-twist structure [13]. These features are well described by the DM interaction in the following shape:

$$H_{DM} = D\hat{r}_{ij} \cdot (\mathbf{S}_i \times \mathbf{S}_j); \quad (11)$$

namely, the DM vector  $\mathbf{D}$  in Eq. (1) should point from one spin to the other. Although it is compatible with the symmetry [31], the microscopic origin is still lacking. However, it can be understood by the SOC in our effective Hamiltonian as follows.

Quantitatively, we can employ the field approach to calculate the Ruderman-Kittel-Kasuya-Yosida (RKKY) interaction between two neighboring spins  $\mathbf{S}_1$  and  $\mathbf{S}_2$  [32–34]. The electron's action is given by

$$S = \sum_n \int d^3\mathbf{k} \bar{\psi}(-\mathbf{k}, -i\omega_n) \times \left( -i\omega_n + \frac{\mathbf{k}^2}{2m} + \alpha\mathbf{k} \cdot \boldsymbol{\sigma} \right) \psi(\mathbf{k}, i\omega_n) + \sum_{i=1}^2 \sum_n \int d^3\mathbf{k} \bar{\psi}(-\mathbf{k} - \mathbf{q}, -i\omega_n) \mathbf{S}_i \cdot \boldsymbol{\sigma} e^{-i\mathbf{q} \cdot \mathbf{R}_i} \psi(\mathbf{k}, i\omega_n), \quad (12)$$

where  $\mathbf{R}_i$  are the positions of two spins. The spin interaction can be derived by integrating out the electrons using the gradient expansion. Up to the second order, the spin-spin interaction is given by

$$S_{\text{eff}} = -2 \sum_n \int d^3\mathbf{k} \text{Tr} [G(\mathbf{R}, i\omega_n) \mathbf{S}_1 \cdot \boldsymbol{\sigma} G(-\mathbf{R}, i\omega_n) \mathbf{S}_2 \cdot \boldsymbol{\sigma}], \quad (13)$$

where  $\mathbf{R} = \mathbf{R}_1 - \mathbf{R}_2$  and  $G(\mathbf{R}, i\omega_n)$  is the real-space Green's function, defined as

$$G(\mathbf{R}, i\omega_n) = \int d^3\mathbf{k} \frac{e^{-i\mathbf{k} \cdot \mathbf{R}}}{-i\omega_n + \frac{\mathbf{k}^2}{2m} - \alpha\mathbf{k} \cdot \boldsymbol{\sigma}} \quad (14)$$

$$= \int_0^\infty dk \int_0^\pi d\theta k^2 \sin\theta \int_0^{2\pi} d\varphi \frac{i\omega_n - \frac{k^2}{2m} + \alpha\mathbf{k} \cdot \boldsymbol{\sigma}}{(-i\omega_n + \frac{k^2}{2m})^2 - \alpha^2 k^2} e^{-i\mathbf{k} \cdot \mathbf{R}}. \quad (15)$$

One can decompose the momentum  $\mathbf{k}$  into directions parallel and perpendicular to  $\hat{R}$  as  $\mathbf{k} = (\mathbf{k} \cdot \hat{R})\hat{R} + (\hat{R} \times \mathbf{k}) \times \hat{R} \equiv \mathbf{k}_{\parallel} + \mathbf{k}_{\perp}$ . Apparently, because  $\mathbf{k}_{\perp} \cdot \mathbf{R} = 0$ ,  $\exp(i\mathbf{k}_{\perp} \cdot \mathbf{R}) = 1$ , and

$$\int_0^{2\pi} d\varphi \frac{\alpha\mathbf{k}_{\perp} \cdot \boldsymbol{\sigma}}{(-i\omega_n + \frac{k^2}{2m})^2 - \alpha^2 k^2} = 0. \quad (16)$$

The only contribution comes from the coupling between the  $\mathbf{k}_{\parallel}$  and Pauli matrices. Thus,

$$\begin{aligned} G(\mathbf{R}, i\omega_n) &= \int_0^\infty dk \int_0^\pi d\theta k^2 \sin\theta \\ &\quad \times \int_0^{2\pi} d\varphi \frac{i\omega_n - \frac{k^2}{2m} + \alpha \mathbf{k}_{\parallel} \cdot \boldsymbol{\sigma}}{\left(-i\omega_n + \frac{k^2}{2m}\right)^2 - \alpha^2 k^2} e^{-i\mathbf{k}_{\parallel} \cdot \mathbf{R}} \\ &= 2\pi \int_0^\infty dk \int_0^\pi d\theta k^2 \sin\theta \\ &\quad \times \frac{i\omega_n - \frac{k^2}{2m} + \alpha k \cos\theta \hat{R} \cdot \boldsymbol{\sigma}}{\left(-i\omega_n + \frac{k^2}{2m}\right)^2 - \alpha^2 k^2} e^{-ikR \cos\theta} \\ &\equiv G_0(R) + G_1(R) \mathbf{R} \cdot \boldsymbol{\sigma}, \end{aligned} \quad (17)$$

where

$$G_0(R) = 2\pi \int_0^\infty dk \int_0^\pi d\theta \frac{k^2 \sin\theta \left(i\omega_n - \frac{k^2}{2m}\right)}{\left(-i\omega_n + \frac{k^2}{2m}\right)^2 - \alpha^2 k^2} e^{-ikR \cos\theta} \quad (18)$$

and

$$G_1(R) = \frac{2\pi}{R} \int_0^\infty dk \int_0^\pi d\theta \frac{\alpha k^3 \sin\theta \cos\theta}{\left(-i\omega_n + \frac{k^2}{2m}\right)^2 - \alpha^2 k^2} e^{-ikR \cos\theta}. \quad (19)$$

One can easily get these Green's functions by evaluating contour integrals. The real part of the poles of  $k$  gives rise to the Friedel oscillations.

Consequently, the effective RKKY Hamiltonian is given by

$$\begin{aligned} H^{\text{RKKY}} &= -\frac{2}{\beta} \sum_n [(G_0^2 + G_1^2) \mathbf{S}_1 \cdot \mathbf{S}_2 \\ &\quad + 2G_0 G_1 \mathbf{R} \cdot (\mathbf{S}_1 \times \mathbf{S}_2)]. \end{aligned} \quad (20)$$

The first term is the Heisenberg exchange, while the second term is the DM interaction. The DM vector  $\mathbf{D}$  in Eq. (1) is along  $\mathbf{R} = \mathbf{R}_1 - \mathbf{R}_2$ , which is consistent with Eq. (11) for B20 compounds. One can easily show that even if the cubic spin-orbit coupling in Eq. (10) is included, the direction of DM vector is still unchanged. Thus, the SOC in Eq. (10) gives rise to the right DM interactions in B20 and therefore the right physical origin. In the next two sections, we will discuss the effects of these two SOC terms in the collective transports.

The physical picture behind this calculation is the following. By the linear spin-orbit coupling  $\alpha \mathbf{k} \cdot \boldsymbol{\sigma}$ , the conduction electron effectively feels a magnetic field  $-\alpha \mathbf{k} \sim -\alpha m \mathbf{v} / \hbar$ . Therefore, once it hops from one site to the other, its spin must precess about the effective magnetic field along the joint line between these two sites. The coupling between the conduction electron and local magnetic moments thus reduces the energy once the moments at these two sites precess in the same way. The direction of the DM vector  $\mathbf{D}$  is thus parallel to the effective field, which points one spin to the other.

In reality, the interaction between the neighboring spins might have various origins besides the RKKY mechanism. However, the physical picture of spin precession persists in any mechanism. Therefore, the DM interaction always has the desired form once the spin-orbit coupling, Eq. (10), is present.

An interesting consequence follows when an ultrathin film of a B20 compound is grown along the [001] direction and an electric field is applied perpendicular to the film. The intrinsic linear SOC gives  $H = \alpha(k_x \sigma_x + k_y \sigma_y)$ , while the additional Rashba SOC induced by the electric field is  $H = \alpha_R(k_x \sigma_y - k_y \sigma_x)$ . Still the intrinsic SOC gives DM interactions with the DM vector pointing from one spin to the neighbor on the film. However, the Rashba SOC contributes a DM vector perpendicular to the intrinsic one. In B20 compounds the spin helix looks like a successive array of Bloch domain walls, where the spins are rotating in a plane perpendicular to the propagation direction. However, in the large  $\alpha_R$  limit, the resulting spin helix is a successive array of Neel walls, where the spins are coplanar to the propagation direction. Therefore, by increasing the electric field, one can expect a gradual deformation of the spin helix. Similarly, the skyrmion will deform to that generated by interfacial DM interactions [35]. These deformations can be observed by Lorentz TEM images.

#### IV. INVERSE SPIN-GALVANIC EFFECT

There have been extensive discussions on the interaction between the conduction electrons and local magnetic moments  $\mathbf{M}$  in metallic magnets. These two are directly coupled to each other via Hund's rule coupling  $H = -J_H \mathbf{M} \cdot \boldsymbol{\sigma}$ , where  $\boldsymbol{\sigma}$  is the spin of the conduction electron. In the adiabatic limit,  $J_H \rightarrow \infty$ , electron spins are parallel to the local moments. Algebraically, one can perform an  $SU(2)$  transformation  $U$  such that  $U^\dagger \mathbf{M} \cdot \boldsymbol{\sigma} U = \sigma_z$ . In the adiabatic limit, only the up spin, namely, the upper left part of the transformed Hamiltonian, is relevant. In the case where moments are spatially nonuniform, the same  $U$  rotation transforms the kinetic energy  $\mathbf{k}^2/2m$  to  $(\mathbf{k} - e\mathbf{A})^2/2m$ , where the  $SU(2)$  gauge field  $e\mathcal{A}_\mu = -iU^\dagger \partial_\mu U$  [36], whose upper left part  $\mathbf{A}$  is the real-space emergent electromagnetic field [17]. The minimal coupling between  $\mathbf{A}$  and the electric current  $\mathbf{j}$  results in the current-driven domain wall or the skyrmion motions [17,37].

The scenario above is no longer valid in the presence of the SOC. Due to the noncommutative nature of the Pauli matrices, the conduction electrons feel more than the emergent electromagnetic field  $\mathbf{A}$ , and additional coupling to the electric current needs to be included. Careful analysis is required in the current case.

One can similarly perform an  $SU(2)$  gauge transformation  $U$  to the Hamiltonian

$$H = \frac{1}{2m} \mathbf{k}^2 + \alpha \mathbf{k} \cdot \boldsymbol{\sigma} - J_H M(r) \cdot \boldsymbol{\sigma}, \quad (21)$$

so that  $U^\dagger M(r) \cdot \boldsymbol{\sigma} U = m \sigma_z$ . The first term again gives rise to  $U^\dagger (\mathbf{k}^2/2m) U = (k - e\mathcal{A})^2/2m$ , with  $e\mathcal{A}_\mu = -iU^\dagger \partial_\mu U$ , while the second one is transformed as

$$U^\dagger \mathbf{k} \cdot \boldsymbol{\sigma} U = U^\dagger \sigma_\mu U (k_\mu - e\mathcal{A}_\mu). \quad (22)$$

In the adiabatic limit, we take the upper left ( $\uparrow\uparrow$ ) part of the transformed Hamiltonian, so that

$$H = \frac{1}{2m} (\mathbf{k} - e\mathbf{A})^2 + \alpha(\mathbf{f} \cdot \mathbf{k} - g) - J_H m, \quad (23)$$

where  $f_\mu = [U^\dagger \sigma_\mu U]_{\uparrow\uparrow}$  and  $g = [\mu U^\dagger \sigma_\mu U e \mathcal{A}_\mu]_{\uparrow\uparrow}$ . As  $\dot{\mathbf{x}} = \frac{\partial H}{\partial \mathbf{k}} = \frac{1}{m}(\mathbf{k} - e\mathbf{A}) + \alpha \mathbf{f}$ , the Lagrangian is given by

$$\begin{aligned} L &= \mathbf{k} \cdot \dot{\mathbf{x}} - H \\ &= \frac{1}{2} m \dot{\mathbf{x}}^2 + e\mathbf{A} \cdot (\dot{\mathbf{x}} - \alpha \mathbf{f}) - m\alpha \mathbf{f} \cdot \dot{\mathbf{x}} + \frac{1}{2} m \alpha^2 \mathbf{f}^2 + \alpha g. \end{aligned} \quad (24)$$

The electric current  $\mathbf{j} = e\dot{\mathbf{x}}$  thus minimally couples to  $(\mathbf{A} - \frac{m\alpha}{e}\mathbf{f})$ , instead of  $\mathbf{A}$  in the absence of the SOC. For local magnetizations  $\hat{m} = (\sin\theta \cos\phi, \sin\theta \sin\phi, \cos\theta)$ , let  $U = u_0 + i\mathbf{u} \cdot \boldsymbol{\sigma}$ . Up to a gauge, we get  $u_0 = \frac{1}{2\sin(\theta/2)}$ ,  $\mathbf{u} = \frac{1}{2\sin(\theta/2)}\hat{z} \times \hat{m}$ , and, consequently,  $\mathbf{f} = \hat{m}$ . The effective coupling between magnetization and the current is thus given by

$$L_c = \frac{1}{e} \mathbf{j} \cdot (e\mathbf{A} - \alpha \mathbf{m}). \quad (25)$$

By varying the total action, the magnetization dynamics obeys the following equation of motion:

$$\dot{\mathbf{m}} + \frac{1}{e} \mathbf{j} \cdot \nabla \mathbf{m} - \frac{\alpha}{e} \mathbf{m} \times \mathbf{j} + \mathbf{m} \times \mathbf{H}_{\text{eff}} = 0. \quad (26)$$

The third term is the contribution from SOC. It shows explicitly that via SOC, an electric current  $\mathbf{j}$  serves as an effective planar field acting on the magnetizations, manifesting the inverse spin-galvanic effect.

The physics of the inverse spin-galvanic effect is very simple. Under a steady electric current, the Fermi surface acquires a shift along the current direction and ends up with a nonvanishing average momentum ( $\mathbf{k}$ ) in the same direction. The SOC  $\alpha \mathbf{k} \cdot \boldsymbol{\sigma}$  thus reduces energy when the spin ( $\boldsymbol{\sigma}$ ) is antiparallel to  $\mathbf{j}$ . This average spin provides a spin-transfer torque on the local magnetizations, which is therefore analogous to an effective magnetic field along  $-\mathbf{j}$ .

Although the effective field along the current will not change routine observables such as the topological Hall effect [19], a physical consequence of this inverse spin-galvanic effect is the current-induced helix reorientations in the helimagnet. It has been shown that the hysteresis under low field is vanishingly small in *B20* compounds [38]. The orientation of the spin helix is completely determined by the direction of external magnetic field. Here we propose that one can use an electric current, instead of magnetic fields, to orient the spin helix. The helix would propagate in parallel with the current, which can be experimentally confirmed by neutron scattering. This effect also applies in *B20* thin films, in which the Lorentz TEM would be a proper way to detect it.

## V. HELICAL RESISTANCE

The SOC has various consequences in the magnetoresistances. Under a low external magnetic field, the ground state of *B20* is the helical state, assembling a successive arrays of magnetic domains. The domain-wall resistance originating from collective spin scattering has been extensively studied both experimentally and theoretically in the context of conventional ferromagnets. SOC would apparently alter the spin scattering and leads to unconventional helical resistance in *B20* compounds.

We consider the Hamiltonian in Eq. (10) while including the Zeeman term  $\boldsymbol{\sigma} \cdot \mathbf{h}$ :

$$\begin{aligned} H &= \frac{k^2}{2m} - \mu + \mathbf{h} \cdot \boldsymbol{\sigma} + \alpha \mathbf{k} \cdot \boldsymbol{\sigma} + \beta [k_x(k_y^2 - k_z^2)\sigma_x \\ &\quad + k_y(k_z^2 - k_x^2)\sigma_y + k_z(k_x^2 - k_y^2)\sigma_z] \end{aligned} \quad (27)$$

$$U(\mathbf{r}) = \frac{1}{N} \sum_i (v I_{2 \times 2} - j\mathbf{h} \cdot \boldsymbol{\sigma}) \delta_{\mathbf{r}, \mathbf{R}_i}. \quad (28)$$

Here  $\mathbf{h}$  is the local magnetization. It rotates in the *yz* plane perpendicular to *x*, the propagation direction.  $U$  is the impurity potential, including both the scalar potential  $v$  and the spin-dependent potential  $-j\mathbf{h} \cdot \boldsymbol{\sigma}$  [39]. In the domain wall, the direction of magnetization is nonuniform. Under the assumption of a slowly varying spin configuration (the helix period  $d \gg 1/k_f$ ), one can perform an  $SU(2)$  gauge transformation  $R$  to the Hamiltonian so that the spin in the domain wall points along the  $\hat{e}_z$  direction.  $R$  is set to

$$R = \exp[-i\theta(x)\sigma_x], \quad (29)$$

with  $\theta(x) = 2\pi x/d$ , where  $d$  is the helix period. By this rotation,

$$\begin{aligned} R^{-1}(\boldsymbol{\sigma} \cdot \hat{h})R &= \sigma_z, \\ R^{-1} \frac{\hbar^2 \nabla^2}{2m} R &= \frac{\hbar^2 \nabla^2}{2m} - i \frac{\hbar^2}{2m} \sigma_x (\partial_x \theta) \partial_x \\ &= \frac{\hbar^2 \nabla^2}{2m} - i \frac{\pi \hbar^2}{md} \sigma_x \partial_x, \\ R^{-1} \sigma_x \partial_x R &= -i \frac{\pi}{d} + \sigma_x \partial_x, \\ R^{-1} \sigma_y \partial_y R &= (\cos\theta \sigma_y - \sin\theta \sigma_z) \partial_y, \\ R^{-1} \sigma_z \partial_z R &= (\cos\theta \sigma_z + \sin\theta \sigma_y) \partial_z. \end{aligned}$$

The cubic SOC terms are transformed in a more complicated way. However, under the large-helix-period approximation,  $d \gg 1/k_f$ , with  $k_f$  being the Fermi wave vector, it can be simplified as

$$\begin{aligned} R^{-1} \sigma_x k_x (k_y^2 - k_z^2) R &\approx \sigma_x k_x (k_y^2 - k_z^2), \\ R^{-1} \sigma_y k_y (k_z^2 - k_x^2) R &\approx (\sigma_y \cos\theta - \sigma_z \sin\theta) k_y (k_z^2 - k_x^2), \\ R^{-1} \sigma_y k_z (k_x^2 - k_y^2) R &\approx (\sigma_z \cos\theta + \sigma_y \sin\theta) k_z (k_x^2 - k_y^2). \end{aligned}$$

To calculate the helical conductivity, we solve the Boltzmann equation with a perturbation method. The deviation of the electron distribution function from the equilibrium one  $f_1 = f - f_0$  is expanded in terms of the spherical harmonic functions  $Y_l^m(\theta, \phi)$  up to  $l = 5$ . The details of the calculation can be found in the Supplemental Material [40].

Figure 1 shows the ratio between the longitudinal resistivities with the current perpendicular to the domain wall (CPW) and the current in the domain wall (CIW). It is found that the ratio is strongly suppressed by the presence of the SOC. In addition, the presence of cubic SOC terms only quantitatively changes the ratio.

The minimum of the ratio is reached when

$$\alpha = \frac{\pi}{md}. \quad (30)$$

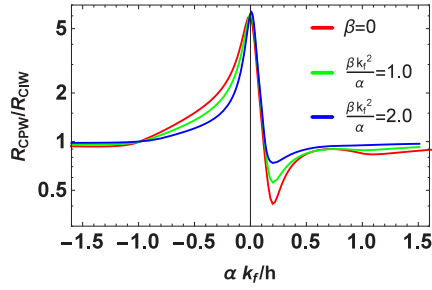


FIG. 1. (Color online) The resistance ratio  $R_{CPW}/R_{CIW}$  vs the spin-orbit coupling. In the plot,  $\pi k_f/(mdh) = 0.2$ ,  $jh/v = 1.06$ . Different curves are for different cubic SOC terms. It is clear that the ratio approaches the one for which the SOC is much larger than the Zeeman energy  $h$ .

To understand this minimum, we consider the Hamiltonian with only the linear SOC coupling, i.e.,  $\beta = 0$ . After the local  $SU(2)$  gauge transformation, the Hamiltonian becomes

$$H = H_0 + V + \text{const}, \quad (31)$$

$$\begin{aligned} H_0 &= \frac{p^2}{2m} - h\sigma_z, \\ V &= \left( \alpha - \frac{\pi}{md} \right) \sigma_x p_x + \alpha \sigma_y (p_y \cos \theta + p_z \sin \theta) \\ &\quad + \alpha \sigma_z (p_z \cos \theta - p_y \sin \theta), \\ \text{const} &= \frac{\pi^2}{8md^2} - \frac{\alpha\pi}{2d}. \end{aligned} \quad (32)$$

To simplify the notation, we define  $\gamma = \alpha - \frac{\pi}{md}$ . If SOC terms  $\alpha k_f$ ,  $\beta k_f^3$  are much smaller than the Zeeman energy, the eigenstate of the Hamiltonian can be solved based on perturbation. In addition, we assume that the impurity scattering is strongly spin dependent, i.e.,  $v \approx jh$ . In this case, the conductivity is dominated by the outer Fermi surface, with its intraband impurity scattering given by

$$|M_{k \rightarrow k'}^{++}|^2 \approx (v + jh)^2 \left[ \frac{\gamma^2 k_x k'_x + \frac{\alpha^2}{2} (k_y k'_y + k_z k'_z)}{4h^2} \right]^2. \quad (33)$$

Here  $+$  is for the outer Fermi surface. When  $\alpha$  vanishes, it is clear that scattering is larger at larger  $k_x$  and  $k'_x$ . The resistivity comes from the fermions with larger momentum along the direction of the current. Therefore,  $\rho_x \gg \rho_{y/z}$ , and thus, the ratio  $R_{CPW}/R_{CIW}$  reaches its maximum. When  $\gamma = 0$  [ $\alpha = \pi/(md)$ ], the scattering rate is larger for larger  $k_{y/z}$  and  $k'_{y/z}$ . Therefore,  $\rho_{y/z} \gg \rho_x$ , and the ratio  $R_{CPW}/R_{CIW}$  reaches the minimum. More detailed information can be found in the Supplemental Material.

## VI. ANOMALOUS ANISOTROPIC MAGNETORESISTANCE

In the previous sections, we have focused mainly on the effects of the linear SOC in Eq. (10). The cubic SOC only slightly modifies these effects. The cubic term fails to bring any qualitative change in these experiments. However, from

the point of view of symmetry, only the cubic SOC breaks the  $C_4$  rotation, and it must give rise to anisotropic behaviors of the magnetoresistance. To this end, we study the case when external magnetic field is sufficiently large to polarize all magnetic moments along its direction and calculate the magnetoresistances. It is well known that for most of the cubic ferromagnets such as Ni, the AMR shows fourfold symmetry when the magnetic field rotates in the plane perpendicular to the current. However, it has already been reported that in  $B20$  compounds such as  $\text{Fe}_{1-x}\text{Co}_x\text{Si}$  [24], the AMR shows anomalous behavior in that only a twofold symmetry is respected. In this section, we will show how the cubic SOC leads to this observation.

The same model as in the previous section is employed. The Hamiltonian and the impurity potential are in the same form as in Eqs. (27) and (28). The conductivity  $\sigma_{zz}(\mathbf{h})$  is calculated while varying the magnetization  $\mathbf{h}$  in the  $x$   $y$  plane. Most of the ferromagnetic materials have high symmetry and respect  $C_4$  symmetry. Thus,  $\sigma_{zz}(h\hat{e}_x) = \sigma_{zz}(h\hat{e}_y)$  in these cases. However, due to the  $C_4$  breaking in  $B20$  compounds, the anomalous AMR is expected where the ratio between the conductivities  $\sigma_{zz}(h\hat{e}_x)$  and  $\sigma_{zz}(h\hat{e}_y)$  deviates from 1.

Before performing the calculation, let's explore the symmetries of the Hamiltonian in Eq. (27). It is found that

$$H(\alpha, \beta, h\hat{e}_y) = SH(\alpha, -\beta, h\hat{e}_x)S^{-1}. \quad (34)$$

Here  $S$  is the operator which rotates the system along the  $z$  axis by  $\pi/2$ . Therefore,

$$\sigma_{zz}(\alpha, \beta, h\hat{e}_x) = \sigma_{zz}(\alpha, -\beta, h\hat{e}_y). \quad (35)$$

In addition, the conductivity is invariant under the space-inversion symmetry  $P$ ,

$$\begin{aligned} H(-\alpha, -\beta, \mathbf{h}) &= PH(\alpha, \beta, \mathbf{h})P^{-1} \implies \sigma_{zz}(\alpha, \beta, \mathbf{h}) \\ &= \sigma_{zz}(-\alpha, -\beta, \mathbf{h}). \end{aligned} \quad (36)$$

Combining Eqs. (35) and (36), we conclude

$$\sigma_{zz}(\alpha, \beta, h\hat{e}_x) = \sigma_{zz}(\alpha, -\beta, h\hat{e}_y) = \sigma_{zz}(-\alpha, \beta, h\hat{e}_y). \quad (37)$$

Solely by symmetry argument, it is found that the anomalous AMR, defined as  $\sigma_{zz}(h\hat{e}_x)/\sigma_{zz}(h\hat{e}_y) - 1$ , vanishes if either of the two spin-orbit couplings,  $\alpha$  and  $\beta$ , vanishes. Similarly, we have  $\sigma_{zz}(\alpha, \beta, h\hat{e}_h) = \sigma_{zz}(\alpha, \beta, -h\hat{e}_h)$ .

In this section, the conductivity is calculated in the same way as in the previous section. The Boltzmann equation is solved using the perturbation method. The deviation of the electron distribution function is expanded by spherical harmonic functions up to  $l = 5$ . The anisotropy comes from two different sources. (i) the Fermi surface is anisotropic since the Hamiltonian in Eq. (27) breaks  $C_4$  symmetry. (ii) The eigenstate on the Fermi surface is anisotropic and thus leads to the anisotropic impurity scattering by the spin-dependent potential in Eq. (28).

The energy of the Hamiltonian in Eq. (27) is given by

$$\begin{aligned} \varepsilon_F &= \frac{\hbar^2 k_F^2}{2m} \pm \{ h_z^2 + \alpha^2 (k_x^2 + k_y^2 + k_z^2) \\ &\quad + \beta^2 [k_x^2 (k_y^2 - k_z^2)^2 + k_y^2 (k_z^2 - k_x^2)^2 + k_z^2 (k_x^2 - k_y^2)^2] \\ &\quad + 2h_z k_z [\alpha + \beta (k_x^2 - k_y^2)] \}^{1/2}. \end{aligned} \quad (38)$$

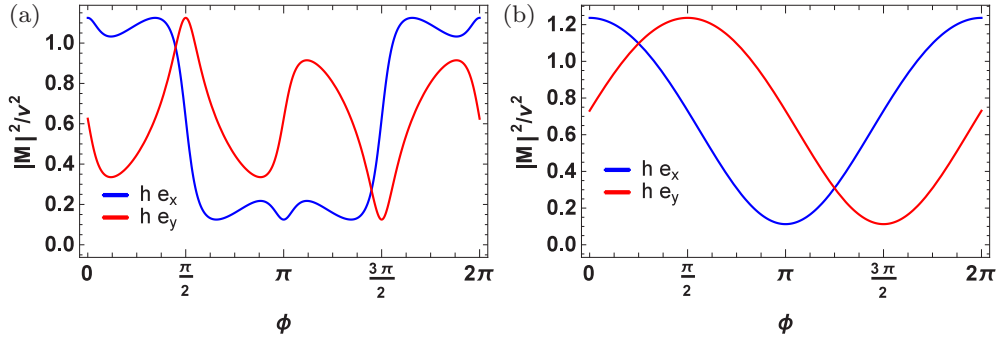


FIG. 2. (Color online) The intraband impurity scattering amplitude from  $(0,0,k_f)$  to  $(k_f \cos \phi, k_f \sin \phi, 0)$  on the outer Fermi surface. Red and blue curves are the scattering magnitude as a function of  $\phi$  when the magnetization field points along  $\hat{y}$  and  $\hat{x}$ , respectively. (a) The Zeeman energy is artificially turned off, while the impurity potential is still spin dependent with  $v/(jh) = 2.0$  and  $\beta k_f^2/\alpha = 1.5$ . The  $C_4$  symmetry is broken in the impurity scattering amplitude. (b)  $\beta = 0$ . Both the Zeeman energy and the impurity spin-dependent potential are nonzero, with  $h/(\alpha k_f) = 0.1$  and  $v/(jh) = 2.0$ . It is clear that  $C_4$  symmetry recovers for  $\beta = 0$ .

The system contains two Fermi surfaces (FSs) since the Kramers degeneracy is lifted. All terms in Eq. (38) respect the symmetry exchanging the indices  $x$  and  $y$  except the last term in the curly braces. Equation (38) shows explicitly that the Fermi-surface asymmetry is possible only when then magnetization is nonzero.

However, the impurity scattering asymmetry is present as long as  $\alpha$  and  $\beta$  are nonzero. Figure 2 shows the intraband scattering magnitude  $|M|^2$  from  $(0,0,k_f)$  to  $(k_f \cos \phi, k_f \sin \phi, 0)$  on the outer Fermi surface. Red and blue curves are  $|M|^2$  as a function of  $\phi$  when the impurity magnetization points along  $\hat{y}$  and  $\hat{x}$ , respectively. If the  $C_4$  symmetry is kept, the blue curve should be the same as the red one after a translation of  $\pi/2$ , which is apparently not the case. It is noticeable that even when the Zeeman field vanishes, the impurity scattering still breaks the  $C_4$  symmetry, although the shape of the Fermi surface is still  $C_4$  symmetric. Of course, in reality, both the Zeeman term and spin-dependent scattering coexist.

Figure 3(a) shows the ratio  $\sigma_{zz}(h\hat{e}_x)/\sigma_{zz}(h\hat{e}_y)$  as a function of the SOC. The ratio is smaller than 1 when  $\alpha$  and  $\beta$  have the same sign and is larger than 1 when two SOC's have different signs. This is consistent with the conclusion [Eq. (37)] derived by symmetry arguments. In addition, it is found that the anomalous AMR vanishes when either  $\alpha = 0$  or  $\alpha \rightarrow \infty$ .

The latter implies that the anomalous AMR vanishes when  $\beta \rightarrow 0$ . This result agrees with our physical picture based on the Fermi-surface topology.  $C_4$  symmetry is restored on the Fermi surface when  $\beta \rightarrow 0$ .

Figure 3(b) shows the anomalous AMR as a function of the magnetization field  $h$ . When  $h$  vanishes, not only does the Zeeman energy vanish, but also the impurity potential becomes spin independent. Therefore, the impurity scattering becomes  $C_4$  symmetric, as well as the Fermi surface. In this case, anomalous AMR vanishes. Our calculations agree well with the experimental results [24]. When the temperature is raised above the Curie temperature, the anomalous AMR vanishes. This corresponds to the case with vanishing magnetization  $h$ . In another limit when  $h \rightarrow \infty$ , the spin on the Fermi surface is fixed by the Zeeman energy. In this situation, the impurity scattering and Fermi surface become isotropic, and therefore, the anomalous AMR vanishes.

Figure 4 shows the variation of the conductivity  $\sigma_{zz}$  as the direction of the in-plane magnetization field changes. Note that  $\sigma_{zz}$  reaches its minimum (maximum) when the field points along the  $x$  ( $y$ ) direction. In our calculation, this comes from the assumption that two SOC couplings have the same sign. If  $\alpha$  and  $\beta$  have different signs, the minimum (maximum) is reached when  $h$  is along the  $y$  ( $x$ ) axis. This result reproduces the experimental observations in [24].

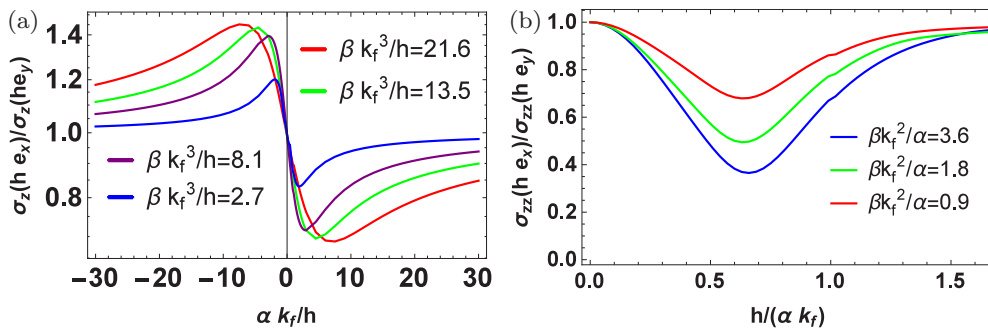


FIG. 3. (Color online) The ratio  $\sigma_z(h\hat{e}_x)/\sigma_z(h\hat{e}_y)$  vs SOC couplings and the magnetization field. (a) The ratio as a function of SOC with  $v/(jh) = 2.0$ . The ratio becomes 1 when  $\alpha = 0$  or  $\beta k_f^2/\alpha \rightarrow 0$ . This agrees with our conclusion in Eq. (37) by symmetry argument. (b) The ratio vs Zeeman energy  $h$  with  $j = 1.0$ . The anomalous AMR vanishes when  $h = 0$  or  $h \rightarrow \infty$ .

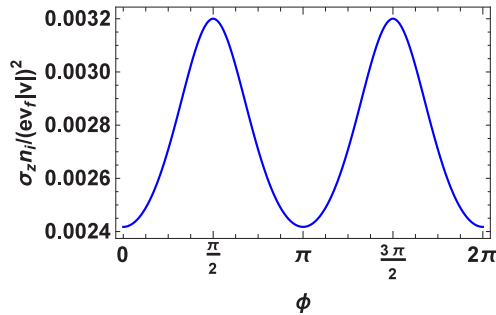


FIG. 4. (Color online) Conductivity vs the direction of the in-plane magnetization field. In the plot,  $\alpha k_f/h = 3.0$ ,  $\beta k_f^3/h = 5.4$ , and  $v/(jh) = 2.0$ .  $n_i$  is the impurity density.

## VII. CONCLUSION

In conclusion, the spin-orbit coupling is the source of various interesting phenomena in *B20* compounds. It not only provides the antisymmetric spin interactions but also

dramatically changes behaviors of the electron transport. The effective Hamiltonian constructed in this work captures the main effects of the SOC in conduction electrons. Despite its simple form, the emergent new physics is closely associated with several experiments. It also calls for many future works to study the spin transports related to this Hamiltonian. First-principles calculations are also encouraged to determine the strength of the SOCs.

## ACKNOWLEDGMENTS

We are grateful for fruitful discussions with C. L. Chien, N. Nagaosa, S. X. Huang, C. X. Liu, O. Tchernyshyov, R. M. Fernandes, V. Galitski, and R. B. Tao. J.K. was supported by the Office of Basic Energy Sciences, U.S. Department of Energy, under Award No. DE-SC0012336. J.Z. was supported by the TIPAC, by the U.S. Department of Energy under Grant No. DEFG02-08ER46544, and by the U.S. National Science Foundation under Grant No. ECCS-1408168.

- 
- [1] Z. Schlesinger, Z. Fisk, H.-T. Zhang, M. B. Maple, J. DiTusa, and G. Aeppli, *Phys. Rev. Lett.* **71**, 1748 (1993).
- [2] J. F. DiTusa, K. Friemelt, E. Bucher, G. Aeppli, and A. P. Ramirez, *Phys. Rev. Lett.* **78**, 2831 (1997).
- [3] S. Mühlbauer, B. Binz, F. Jonietz, C. Pfleiderer, A. Rosch, A. Neubauer, R. Georgii, and P. Böni, *Science* **323**, 915 (2009).
- [4] C. Pfleiderer, D. Reznik, L. Pintschovius, H. v. Löhneysen, M. Garst, and A. Rosch, *Nature (London)* **427**, 227 (2004).
- [5] R. Ritz, M. Halder, M. Wagner, C. Franz, A. Bauer, and C. Pfleiderer, *Nature (London)* **497**, 231 (2013).
- [6] S. X. Huang and C. L. Chien, *Phys. Rev. Lett.* **108**, 267201 (2012).
- [7] X. Z. Yu, N. Kanazawa, Y. Onose, K. Kimoto, W. Z. Zhang, S. Ishiwata, Y. Matsui, and Y. Tokura, *Nat. Mater.* **10**, 106 (2011).
- [8] S. Seki, X. Z. Yu, S. Ishiwata, and Y. Tokura, *Science* **336**, 198 (2012).
- [9] M. Uchida, Y. Onose, Y. Matsui, and Y. Tokura, *Science* **311**, 359 (2006).
- [10] I. Dzyaloshinsky, *J. Phys. Chem. Solids* **4**, 241 (1958).
- [11] T. Moriya, *Phys. Rev.* **120**, 91 (1960).
- [12] T. H. R. Skyrme, *Proc. R. Soc. London, Ser. A* **260**, 127 (1961).
- [13] X. Z. Yu, Y. Onose, N. Kanazawa, J. H. Park, J. H. Han, Y. Matsui, N. Nagaosa, and Y. Tokura, *Nature (London)* **465**, 901 (2010).
- [14] U. K. Röbler, A. N. Bogdanov, and C. Pfleiderer, *Nature (London)* **442**, 797 (2006).
- [15] K. Kadowaki, K. Okuda, and M. Date, *J. Phys. Soc. Jpn.* **51**, 2433 (1982).
- [16] H. Du, J. P. DeGrave, F. Xue, D. Liang, W. Ning, J. Yang, M. Tian, Y. Zhang, and S. Jin, *Nano Lett.* **14**, 2026 (2014).
- [17] J. Zang, M. Mostovoy, J. H. Han, and N. Nagaosa, *Phys. Rev. Lett.* **107**, 136804 (2011).
- [18] T. Schulz, R. Ritz, A. Bauer, M. Halder, M. Wagner, C. Franz, C. Pfleiderer, K. Everschor, M. Garst, and A. Rosch, *Nat. Phys.* **8**, 301 (2012).
- [19] A. Neubauer, C. Pfleiderer, B. Binz, A. Rosch, R. Ritz, P. G. Niklowitz, and P. Böni, *Phys. Rev. Lett.* **102**, 186602 (2009).
- [20] M. Lee, W. Kang, Y. Onose, Y. Tokura, and N. P. Ong, *Phys. Rev. Lett.* **102**, 186601 (2009).
- [21] N. Kanazawa, Y. Onose, T. Arima, D. Okuyama, K. Ohoyama, S. Wakimoto, K. Kakurai, S. Ishiwata, and Y. Tokura, *Phys. Rev. Lett.* **106**, 156603 (2011).
- [22] Y. Li, N. Kanazawa, X. Z. Yu, A. Tsukazaki, M. Kawasaki, M. Ichikawa, X. F. Jin, F. Kagawa, and Y. Tokura, *Phys. Rev. Lett.* **110**, 117202 (2013).
- [23] H. Watanabe, S. A. Parameswaran, S. Raghu, and A. Vishwanath, *Phys. Rev. B* **90**, 045145 (2014).
- [24] S. X. Huang, F. Chen, J. Kang, J. Zang, G. J. Shu, F. C. Chou, and C. L. Chien, [arXiv:1409.7867](https://arxiv.org/abs/1409.7867).
- [25] S. X. Huang, J. Kang, F. Chen, J. Zang, G. J. Shu, F. C. Chou, S. V. Grigoriev, V. A. Dyadkin, and C. L. Chien, [arXiv:1409.7869](https://arxiv.org/abs/1409.7869).
- [26] R. Winkler, *Spin-Orbit Coupling Effects in Two-Dimensional Electron and Hole Systems*, Springer Tracts in Modern Physics (Springer, Berlin, 2003).
- [27] M. S. Dresselhaus, G. Dresselhaus, and A. Jorio, *Group Theory: Application to the Physics of Condensed Matter* (Springer, Berlin, 2010).
- [28] T. Jeong and W. E. Pickett, *Phys. Rev. B* **70**, 075114 (2004).
- [29] G. F. Koster, *Space Groups and Their Representations* (Academic, New York, London, 1957).
- [30] I. Žutić, J. Fabian, and S. Das Sarma, *Rev. Mod. Phys.* **76**, 323 (2004).
- [31] A. O. Leonov, [arXiv:1406.2177](https://arxiv.org/abs/1406.2177).
- [32] M. A. Ruderman and C. Kittel, *Phys. Rev.* **96**, 99 (1954).
- [33] T. Kasuya, *Prog. Theor. Phys.* **16**, 45 (1956).
- [34] K. Yosida, *Phys. Rev.* **106**, 893 (1957).
- [35] A. Fert, V. Cros, and J. Sampaio, *Nat. Nanotechnol.* **8**, 152 (2013).

- [36] Y. B. Bazaliy, B. A. Jones, and S.-C. Zhang, *Phys. Rev. B* **57**, R3213 (1998).
- [37] G. Tatara and H. Kohno, *Phys. Rev. Lett.* **92**, 086601 (2004).
- [38] A. Bauer and C. Pfleiderer, *Phys. Rev. B* **85**, 214418 (2012).
- [39] P. M. Levy and S. Zhang, *Phys. Rev. Lett.* **79**, 5110 (1997).
- [40] See Supplemental Material at <http://link.aps.org/supplemental/10.1103/PhysRevB.91.134401> for technical details on how to obtain the approximate solution of the Boltzmann equation.